Supporting Information

Multifunctional Iron-Cobalt Heterostructure (FeCoHS) Electrocatalyst: Accelerating Sustainable Hydrogen Generation through Efficient Water Electrolysis and Urea Oxidation

Arunagiri Gayathri, Venkatachalam Ashok, Jayaraman Jayabharathi, Dhanasingh Thiruvengadam and Venugopal Thanikachalam*

Department of Chemistry, Material Science Lab, Annamalai University, Annamalai Nagar, Tamil Nadu 608002, India.

Corresponding Author E-mail ID: vtchalam2005@yahoo.com

Contents

SI-I. Experimental section

Materials

Cobalt (II) nitrate $Co(NO_3)_2.6H_2O$, ferrous (II) nitrate $Fe(NO_3)_2.6H_2O$, potassium hydroxide, isopropanol, HCl and ethanol were purchased from SDFCL chemicals and glycerol ($C_3H_8O_3$) was purchased from Avra. Nickel foam was purchased from Vritra Technologies Delhi India. These chemicals were used as received without further purification. Deionized water (DI) was used throughout this reaction.

Synthesis of FeCoHS@NF

400 mg of $Co(NO_3)_2.6H_2O$, 600 mg of $Fe(NO_3)_2.6H_2O$ and 8 mL of glycerol were ground well for 10 minutes in mortar and pestle. The obtained lyophobic sol was called an iron-cobalt glycerate solution. Then 50 ml of water and a piece of pre-cleaned NF were inserted into the reaction mixture. The reaction was carried out at 120°C for 3 h with continuous stirring in a 100 ml solvothermal reactor in an oil bath. The obtained catalyst-grown NF was washed with water to remove the unreacted precursors. Then NF was dried under sunlight for 6 hours. The resultant NF was named iron-cobalt heterostructure (FeCoHS@NF). The obtained left solution was filtered using the standard filtration method, washed and dried with water to remove the unreacted precursors. The resultant residue was named iron-cobalt heterostructure (FeCoHS) and used for comparison purposes. CoHS@NF and FeHS@NF also prepared similar methods without adding $Fe(NO_3)_2.6H_2O$ and $Co(NO_3)_2.6H_2O$, respectively.

Synthesis of FeCoO

To understand the importance of iron-cobalt heterostructure, FeCoHS@NF was calcinated at 350°C in a muffle furnace for 3 h. It leads to the decompose the glycerate and hydroxides from as-prepared FeCoHS@NF and it was called as calcinated FeCoHS@NF. At 350ºC, the decomposition of metal glycerates, hydroxides, oxyhydroxides and removal of interfacial water molecules only takes place, carbonization did not occur <400ºC.

Physical characterization

X-ray diffraction (XRD) of FeCoHS@NF was recorded with Thermo XRD equinox 1000. Fourier transform infrared (FTIR) spectra of FeCoHS@NF were recorded on Shimadzu IR Tracer-100. The morphology of FeCoHS@NF was determined by using a ZEISS Sigma 300 field emission scanning electron microscope (FESEM) operated at 20 kV and elemental mapping was carried out through energy-dispersive X-ray spectroscopy (EDX). JEM-2100 Plus was used to record high-resolution transmission electron microscope (HR-TEM) images of the nanomaterials and a selected area electron diffraction (SAED) pattern was taken from JEM-2100 Plus. The elemental composition of FeCoHS@NF was analyzed by X-ray photoelectron spectroscopy (XPS) with a Kα surface analysis spectrometer.

Electrocatalytic characterization

The catalytic performances of the electrodes for water splitting were studied using a three-electrode configuration connected to a Biologic electrochemical workstation SP-200 potentiostat at room temperature. The FeCoHS@NF was used as the working electrode. The saturated Hg/HgO and graphite rod were used as the reference and counter electrodes, respectively. To remove the surface oxidized layer, a piece of Ni foam (0.5 cm × 0.5 cm) was cleaned through sonication consecutively in 1.0 M HCl, ethanol, and DI water (5 min each) and dried before use as a substrate. Commercially available catalysts (Pt/C & IrO_2) and bare NF were used: about 1.0 mg/ml of commercial Pt/C & IrO_2 suspension was prepared by following a similar methodology for comparison and bare NF was used directly. The commercial Pt/C & IrO_2 catalyst has been used directly as a working electrode without further treatment. All measurements were carried out in 1.0 M KOH. The OER/HER activities of FeCoHS@NF have been analyzed by polarization curves (LSV), electrochemical impedance spectroscopy (EIS) and chronoamperometry. The OER/HER activity of the catalyst has been made by linear sweep voltammetry (LSV) on NF electrode (scan rate: 10 mV s^{-1}). The impedance of the electrocatalyst was measured by electrochemical

impedance spectroscopy (EIS) over a frequency range of 100 kHz to 10 mHz with a sinusoidal perturbation amplitude of 0.4 V. The following table presents the electrolytes used for the different Water Splitting reactions.

Method	Electrolyte
Alkaline Water Electrolysis	1M KOH
Urea-assisted Alkaline Water Electrolysis	1M KOH + 0.33 M Urea (natural Urea concentration in urea-polluted water)
Alkaline Seawater Electrolysis	1M KOH + 0.5 M NaCl (natural NaCl concentration in seawater)
Urea-assisted Seawater Electrolysis	1M KOH + 0.33 M Urea + 0.5 M NaCl (sewage water major contaminants)

SI-II. Calculations

SI-S1. Calculation of Overpotential (η).

The overpotential (η) was determined according to the formula:

$$\eta\ (V) = E\ (RHE) - 1.23\ V \quad (1)$$

SI-S2. Calculation of Tafel plot.

Tafel plots were derived from the LSV curves, and the Tafel slope was calculated using the equation:

$$\eta = a + b \log j \quad (2)$$

where η, a, b, and j refer to the overpotential, exchange current density, Tafel slope, and current density, respectively.

SI-S3. Calculation of Turnover frequency.

Here, the turnover frequency (TOF) rate of evolved molecular O_2/H_2 per surface active site per second can be calculated. The overpotential used for the calculation of TOF was set at a potential of 1.6/-0.25 V vs. RHE. The TOF can be calculated using the equation:

$$\mathbf{TOF = [J \times A / n \times F \times \Gamma]} \quad (3)$$

where, **J** - current density (A cm^{-2}),

A – Electrode surface area,

n - the number of electron transfers required to generate one molecule of the target product (2 for H_2, 4 for O_2, 6 for N_2 and CO_2)

F- faraday constant (96485 C mol^{-1}),

Γ - surface concentration of the active site or the number of atoms participating in the catalytic reaction.

SI-S4. Calculation of EASA.

The calculations of EASA and roughness factor (RF) are based on the following equation:

$$\mathbf{EASA = C_{dl} / C_s} \quad (4)$$

$$\mathbf{RF = EASA / GSA} \quad (5)$$

$$\mathbf{EASA\text{-}normalized\ current\ density = current\ density \times C_s / C_{dl}} \quad (6)$$

In eq (4, 6), C_{dl} is the measured double layer capacitance of samples in 1.0 M KOH (mF), and C_s is the specific capacitance of the catalyst (C_s = 0.04 mF cm^{-2} in 1.0 M KOH). In eq (5), RF is the roughness factor and GSA is the geometric surface area of the material.

SI-S5. Calculation of O_2/H_2 generation

Based on the displaced amount of water due to the O_2/H_2 bubbles, the amount of O_2/H_2 generated was calculated using the following equations

Amount of O_2/H_2 generated in 1 h = amount of water displaced in liters (7)

$$\text{Amount of } O_2/H_2 \text{ generated in moles for 1 h} = \frac{\text{amount of water displaced (liters)}}{22.4 \text{ liters}} \quad (8)$$

We have also calculated the O_2/H_2 generation rate from the electrical charge passed through the electrode using the equation given below.

$$\left(\begin{array}{l}\text{Current obtained} \\ \text{During water electrolysis}\end{array} \text{ X } \begin{array}{l}\text{Time duration for} \\ \text{each potential}\end{array}\right) = \text{Coulomb} \quad (9)$$

$$\frac{\text{Coulomb x F}}{96485C} = \text{No. of moles of } e^- \text{ for } O_2/H_2 \text{ generation} \quad (10)$$

$$\frac{\text{No. of moles of } e^- \text{ for } O_2/H_2 \text{ generation x 1 mole of } O_2/H_2 \text{ gas}}{4/2 \text{ moles of electron}} = \text{Moles of } O_2/H_2 \text{ generated} \quad (11)$$

SI-S6. Calculation of Faradaic Efficiency

At the constant potential of 1.61 V given across the FeCoHS@NF//FeCoHS@NF electrode couples assembled and sealed in H-type full cell in 1.0 M KOH. During the electrolysis, evolved gas molecules were measured by the water displacement method. The applied potential can provide 10 mA cm^{-2} current density to the system and the electrolysis was monitored for 60 min. each 10 minutes of analysis data shown in the data (Figure 8f). Theoretical number of moles of gas molecules can be calculated from Faraday's second law of electrolysis according to the following equation:[2]

$$\mathbf{Vt=Q/nF} \quad (12)$$

where Vt is the number of oxygen and hydrogen molecules calculated theoretically, Q-total charge passed to the cell systems, n-number of electrons (n=4 for O_2 and n=2 for H_2) and F-Faraday constant 96485.3 C/mol.

The Faradaic Efficiency of OER/HER was estimated using the following equation:

$$\mathbf{FE = 4Fn_{O2}/It \times 100\%} \quad (13)$$

$$\mathbf{FE = 2Fn_{H2}/It \times 100\%} \quad (14)$$

Where F is Faraday constant (96485 C/mol), n_{O2} is the number of moles of experimental O_2 during the reaction (mol), n_{H2} is the number of moles of experimental H_2 during the reaction (mol), I is the current of the reaction (A), and t is the reaction time (s).

SI-S7. Calculation of Energy Consumption

According to the Faraday's law, the power consumption for a water electrolysis process can be expressed as follows:[1]

$$Energy\ consumption = v_{cell} \times \frac{nF}{3600} \times \frac{1}{v_m} kWhm^{-3} \quad (15)$$

where the V_{cell} is the voltage during electrolysis, n is the number of electrons (2 for HER), F represents the Faraday constant of 96,485 C mol^{-1}, and V_m is the molar volume of gas to be 24.47 L mol^{-1} at 25 °C and 1 atm. The following table compares power consumption at different current densities for hydrogen production in different electrolyte water-splitting systems.

Methode	**Energy consumed (mA/cm²)**				
	10	**25**	**50**	**75**	**100**
Urea-assisted Alkaline Water Electrolysis	3.06	3.35	3.57	3.74	3.85
Urea-assisted Seawater Electrolysis	3.24	3.52	3.74	3.94	4.13
Alkaline Seawater Electrolysis	3.41	3.72	4.0	4.13	4.27
Alkaline Water Electrolysis	3.47	3.81	4.1	4.22	4.35

SI-S8. Environmental impact assessment

Equation S1

$$Mass\ Intensity\ = \frac{Mass\ of\ all\ reactents\ used\ excluding\ water}{Mass\ of\ product} kg/kg\ product$$

Equation S2

$$Water\ Intensity\ (Wp) = \frac{Mass\ of\ all\ water\ used}{Mass\ of\ product} kg/kg\ product$$

Equation S3

$$Reaction\ Mass\ Efficiency\ (RME) = \frac{Mass\ of\ product}{Mass\ of\ all\ reactents} \times 100\%$$

Equation S4

$$Energy\ Intensity\ = \frac{Amount\ of\ non\ renewable\ energy\ used}{Mass\ of\ product} kW.h/kg$$

Equation S5

$$E\ factor = \frac{[kg(raw\ material) -\ kg(desired\ product)]}{[kg(total\ product\ including\ water)]}$$

SI-III. Figures

Figure S1. XPS survey spectrum of FeCoHS@NF

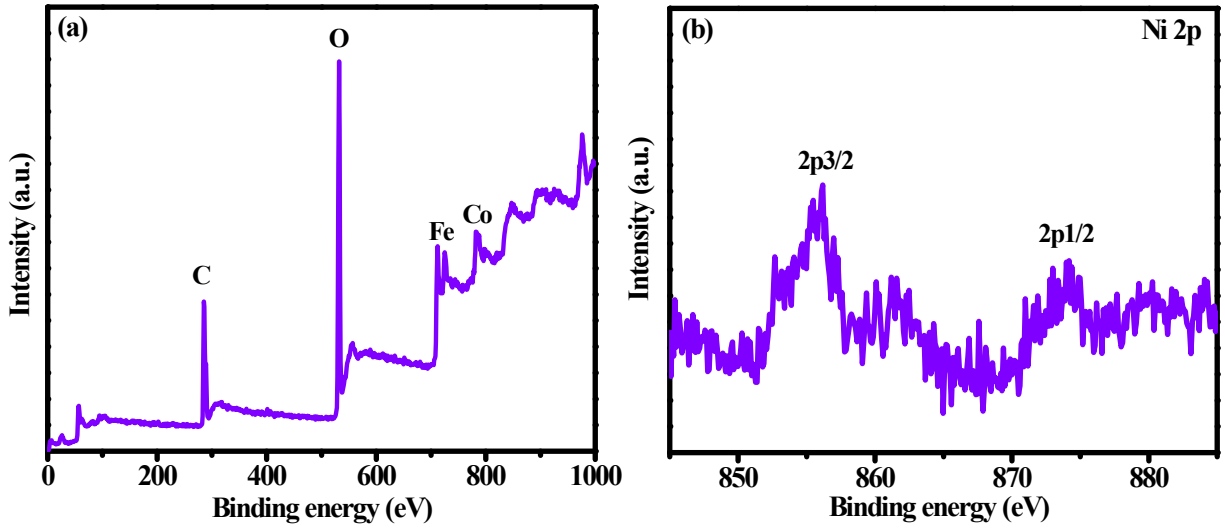

Figure S2. XPS spectrum of FeHS@NF (a-c), XPS spectrum of CoHS@NF (d-f), Fe XPS comparison (g), and Co XPS comparison.

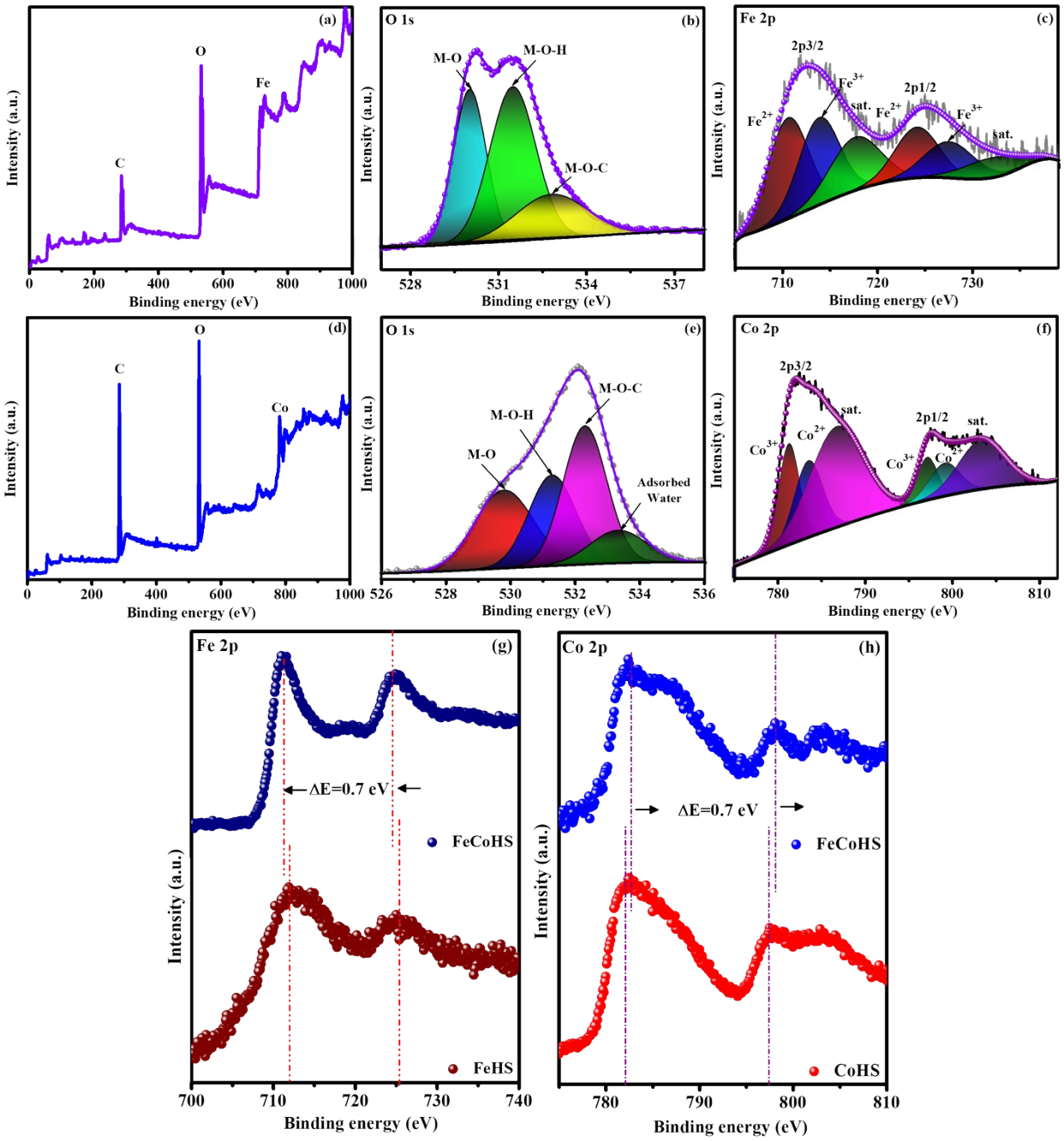

Figure S3. IR spectrum: (a) CoHS@NF, (b) FeHS@NF, and (c) Calcination.

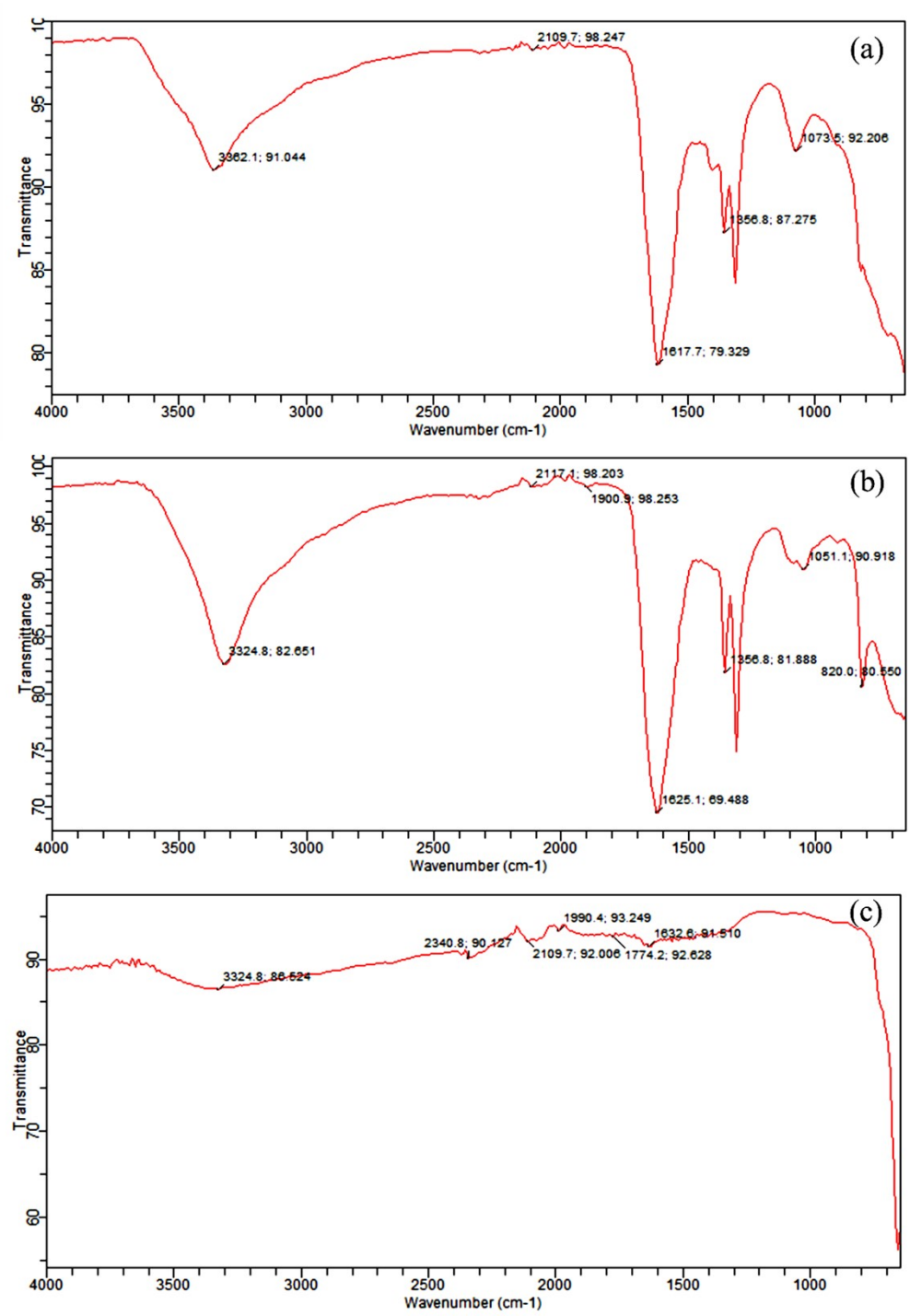

Figure S4. FE-SEM of calcinated FeCoHS: field of view (a); carbon (b); nitrogen (c); oxygen (d); iron (e); nickel (f) and EDX spectrum (g).

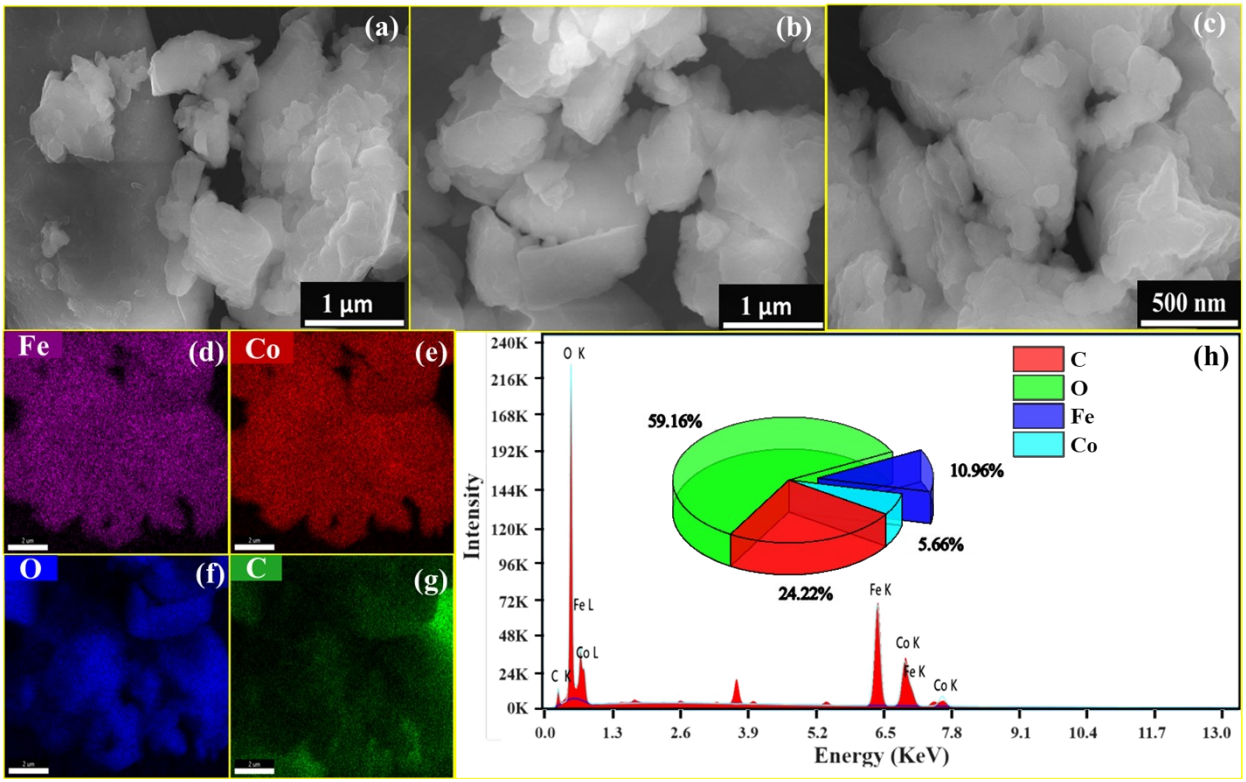

Figure S5. OER CV comparison of electrocatalyst for OER, Full CV and Redox peak up to 10 mV cm^{-2}.

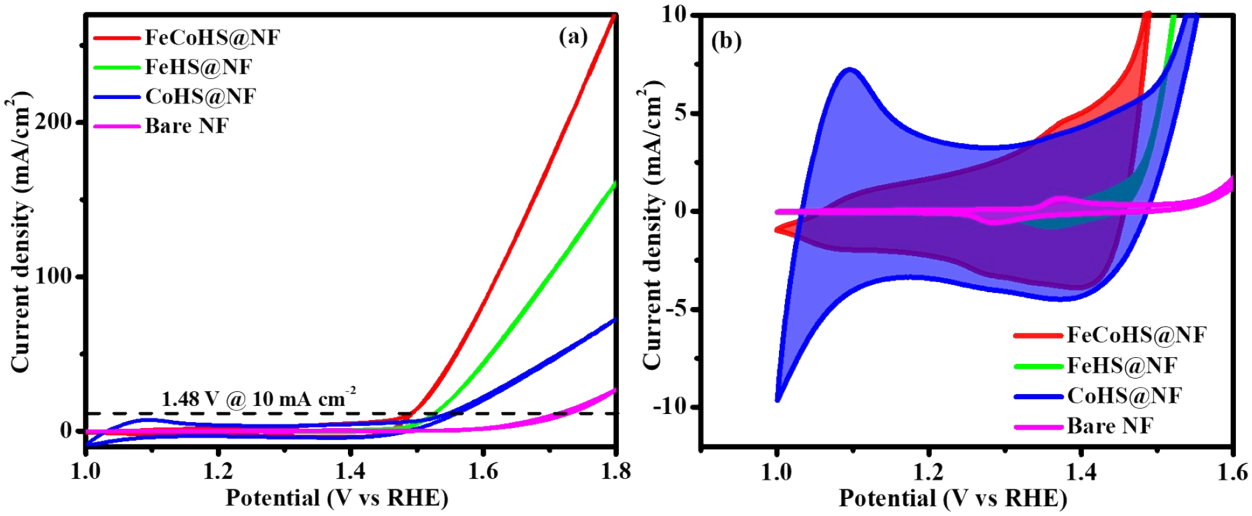

Figure S6. OER ECSA of different electrocatalysts: (a) FeCoHS@NF, (b) FeHS@NF, (c) CoHS@NF and (d) Bare NF.

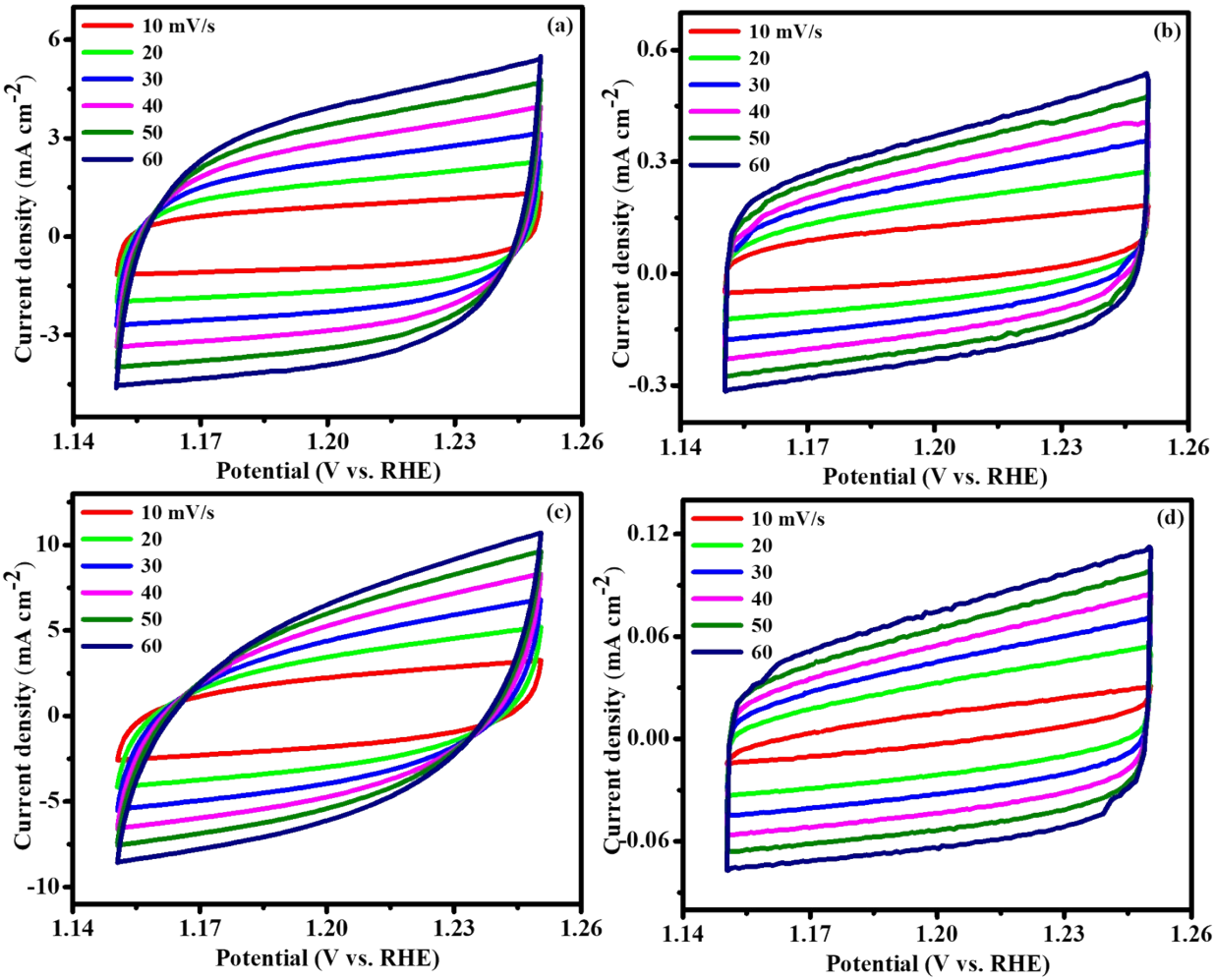

Figure S7. HER ECSA of different electrocatalysts: (a) FeCoHS@NF, (b) FeHS@NF, (c) CoHS@NF and (d) Bare NF.

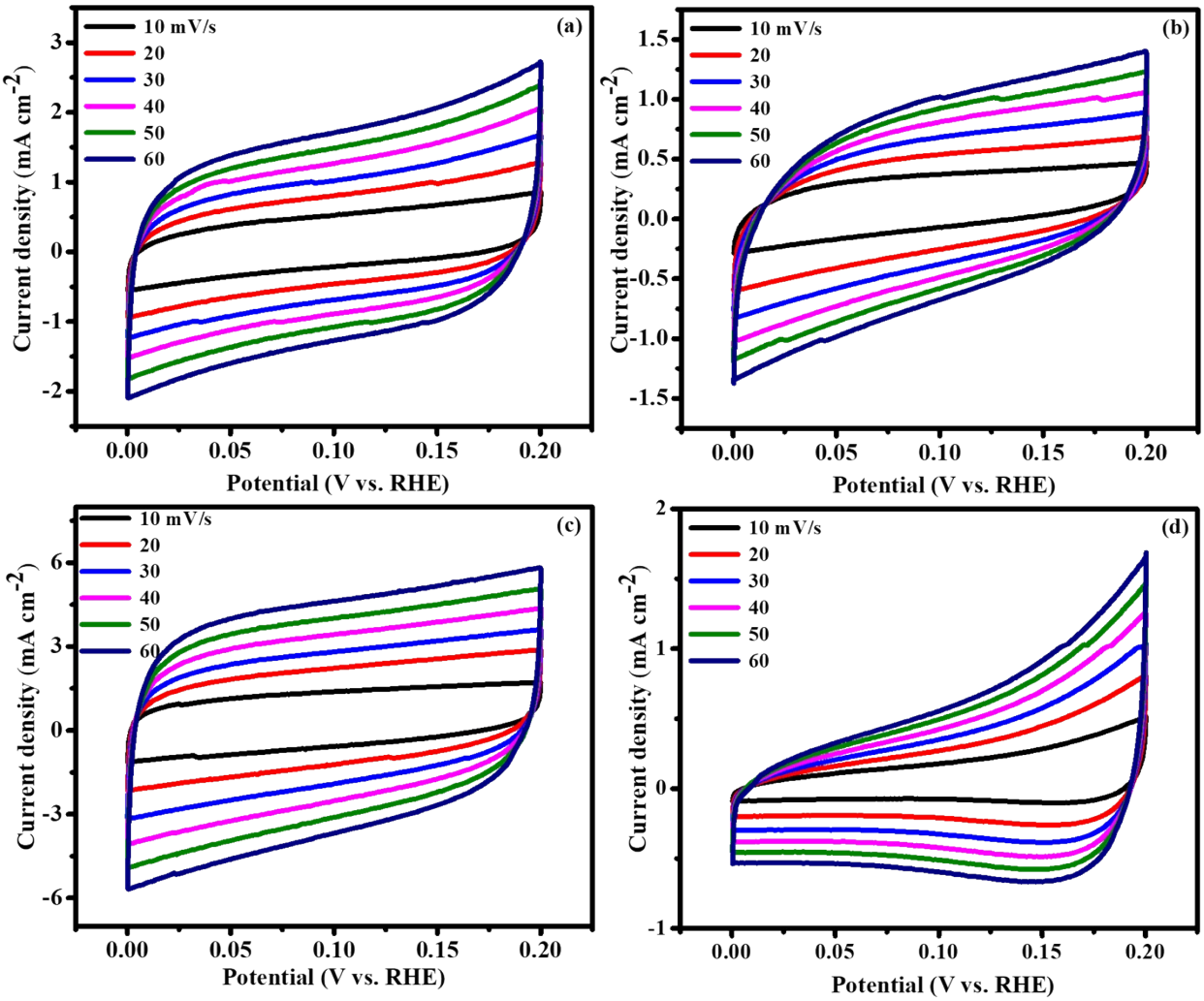

Figure S8. Calculated faradic efficiency for O_2/H_2 generation.

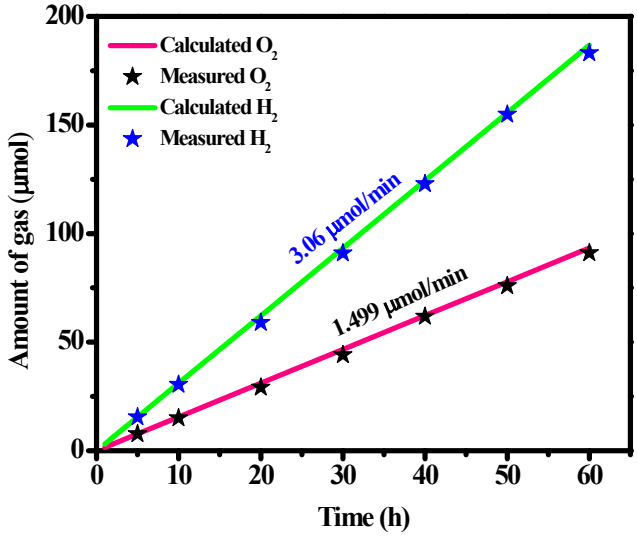

Figure S9. UOR ECSA of different electrocatalysts:(a) FeCoHS@NF, (b) FeHS@NF, (c) CoHS@NF, and (d) Double-layer capacitance .

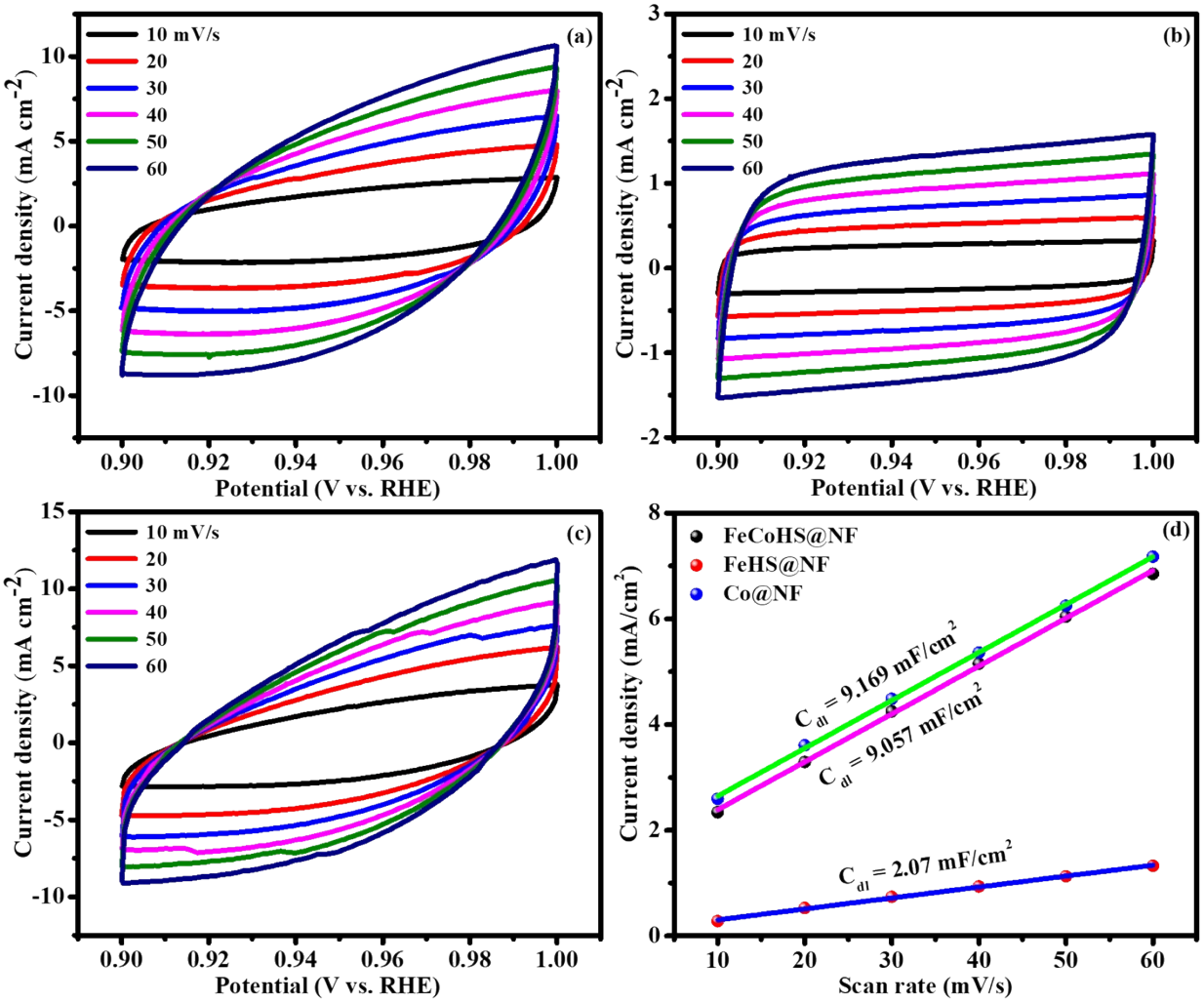

Figure S10. Post FE-SEM image of FeCoHS@NF; after OER (a-c) and after HER (d-f).

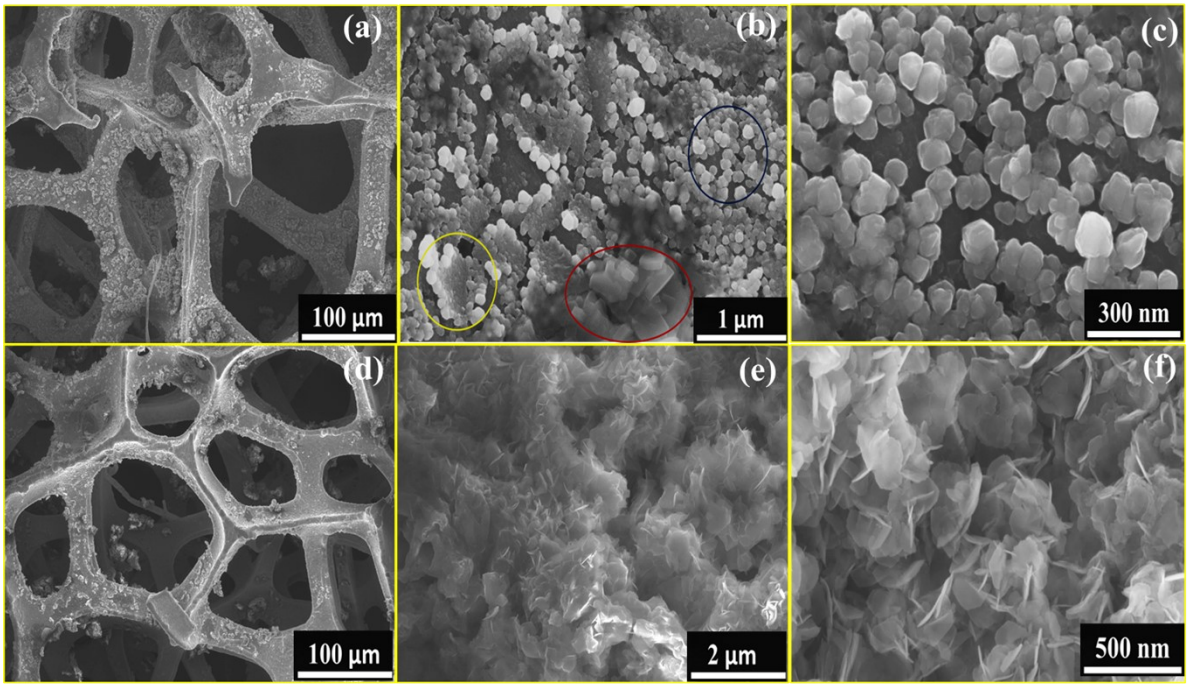

Figure S11. **Post FE-SEM elemental mapping image of FeCoHS@NF after OER: field of view (a); iron (b); cobalt (c); carbon (d); oxygen (e); nickel (f) and EDX spectrum (g).**

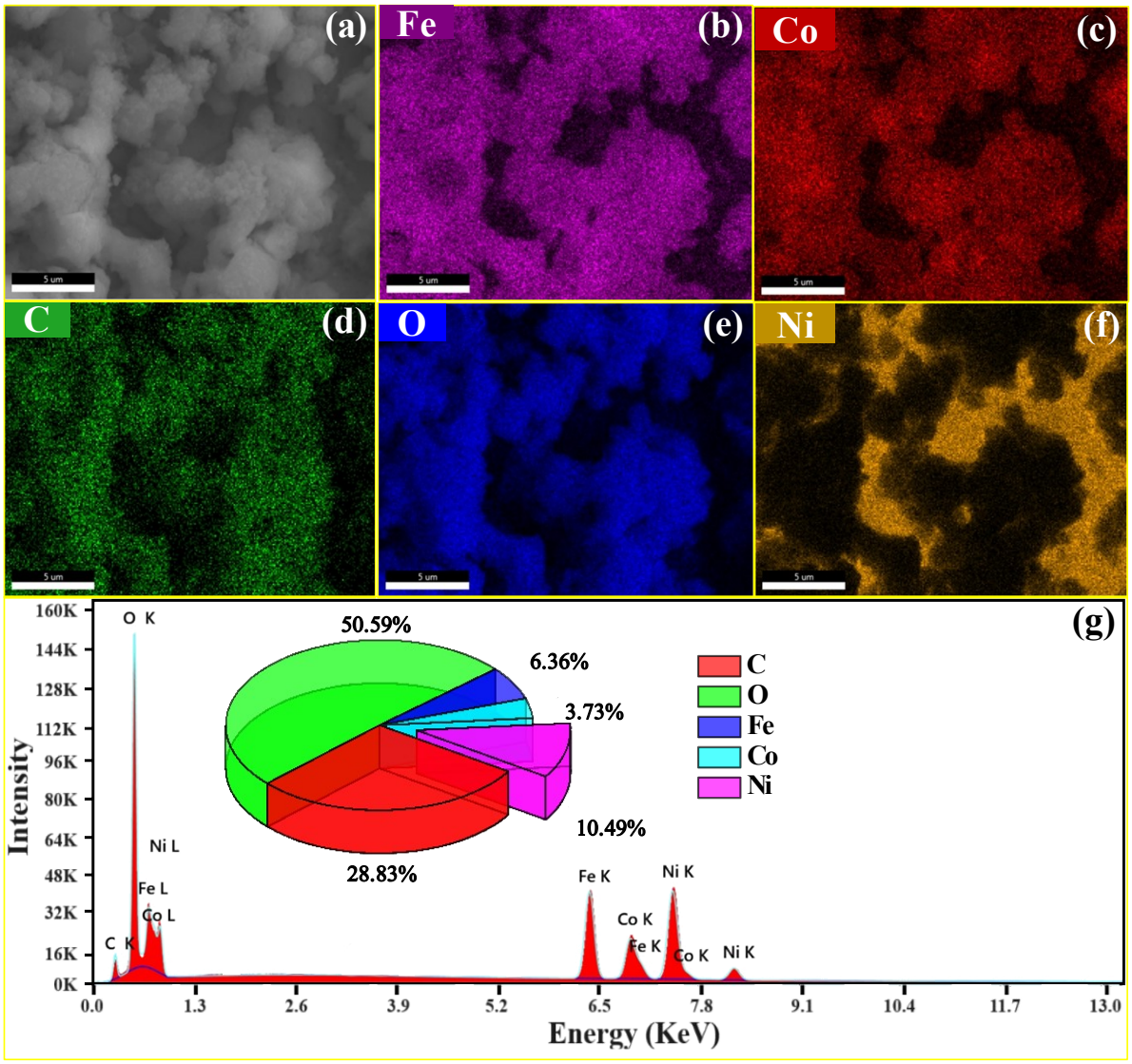

Figure S12. Post FE-SEM elemental mapping image of FeCoHS@NF after HER: field of view (a); iron (b); cobalt (c); carbon (d); oxygen (e); nickel (f) and EDX spectrum (g).

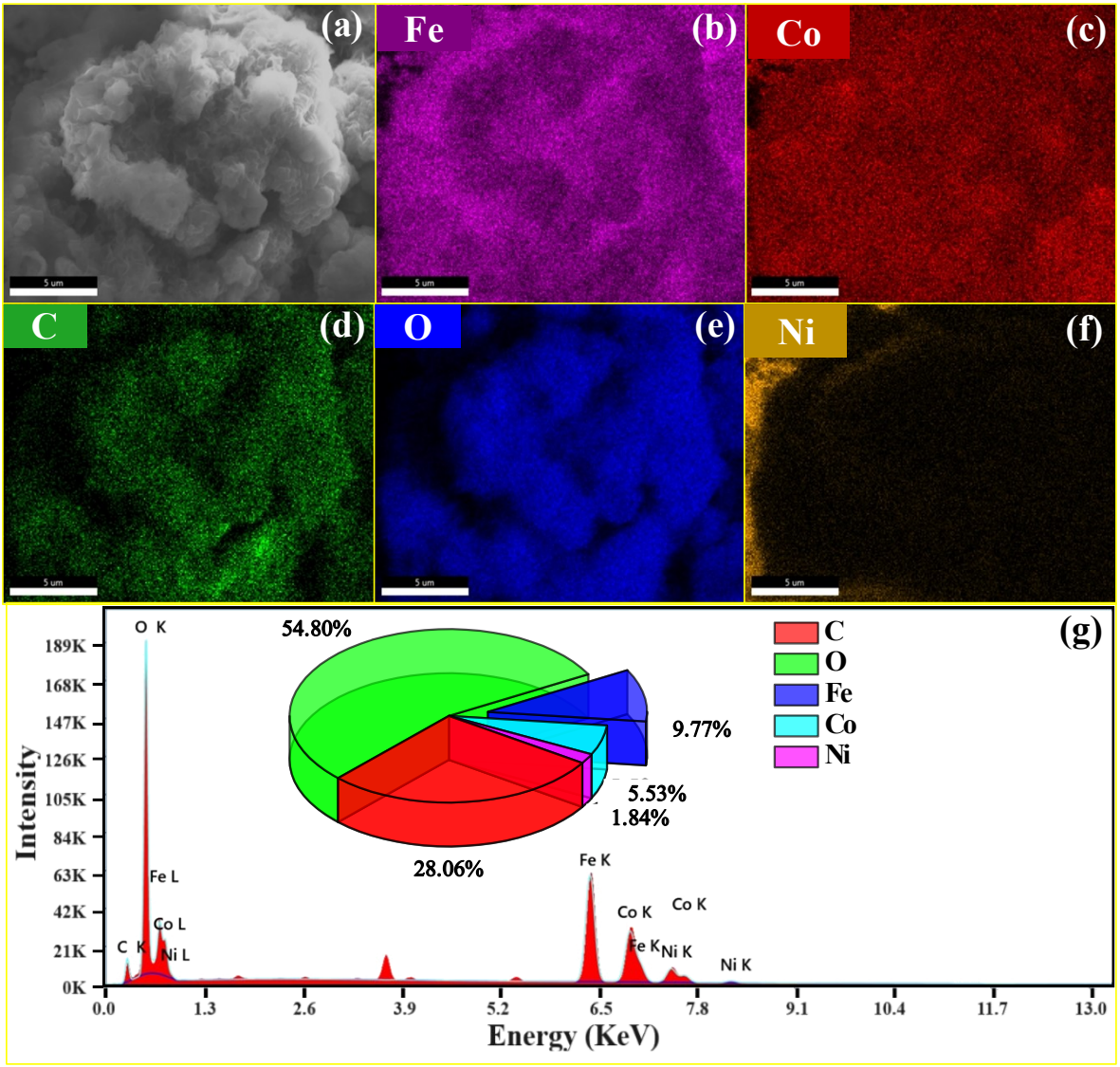

Figure S13. Post FE-SEM image of FeCoHS@NF after UOR stability.

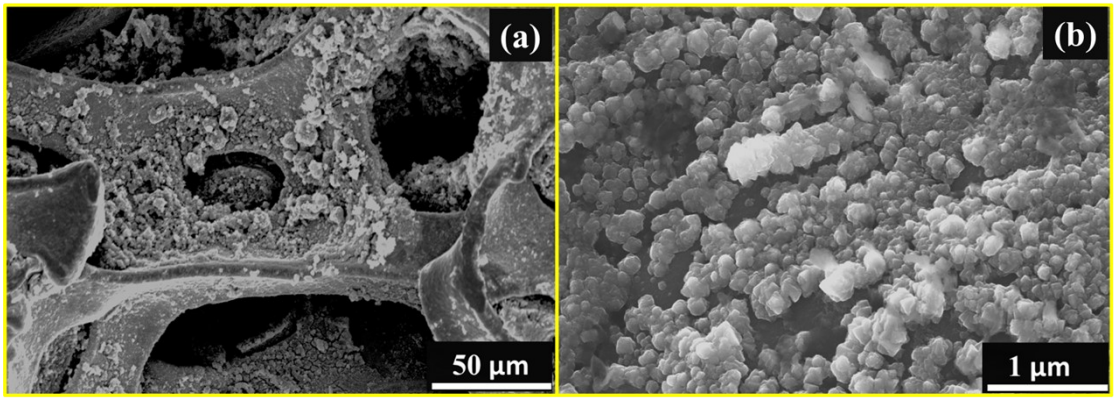

Figure S14. Post FE-SEM image of FeCoHS@NF after stability in alkaline seawater; after OER (a-b) and after HER (c-d).

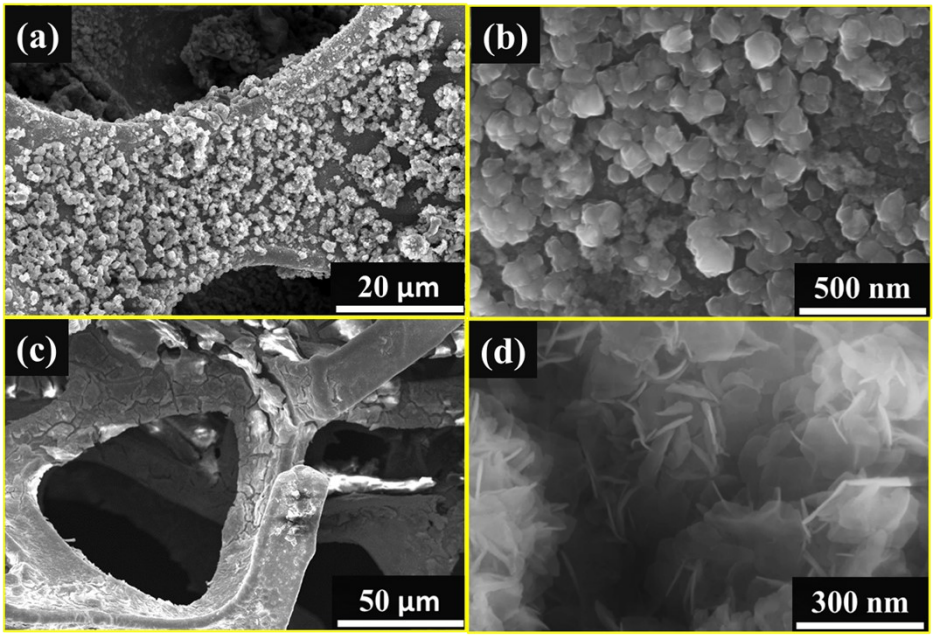

Figure S15. XRD spectra of FeCoHS@NF: (a) After OER, (b) After HER, (c) Bare NF, and (d) After UOR.

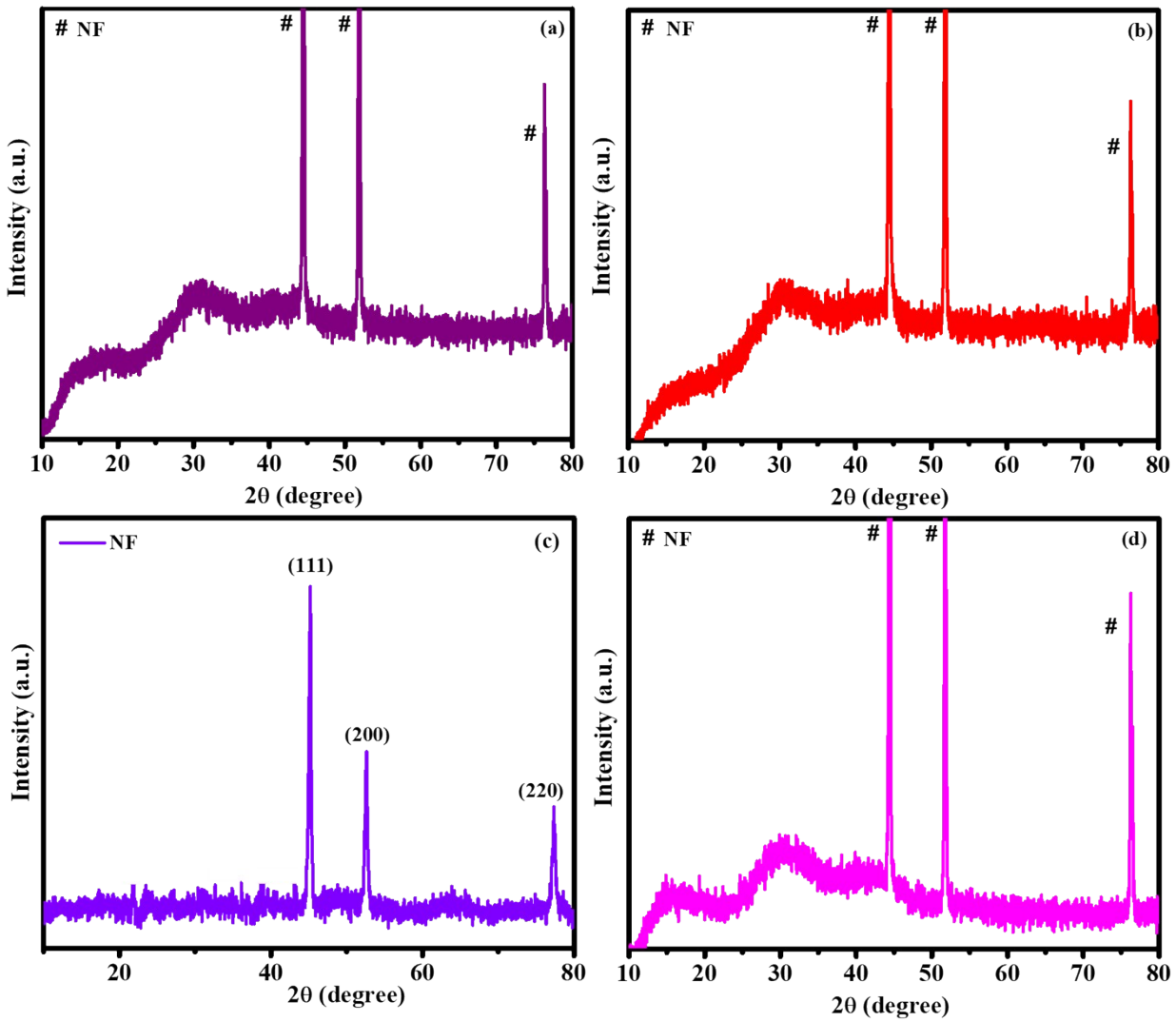

Figure S16. IR spectrum of FeCoHS@NF: (a) After OER and (b) After HER.

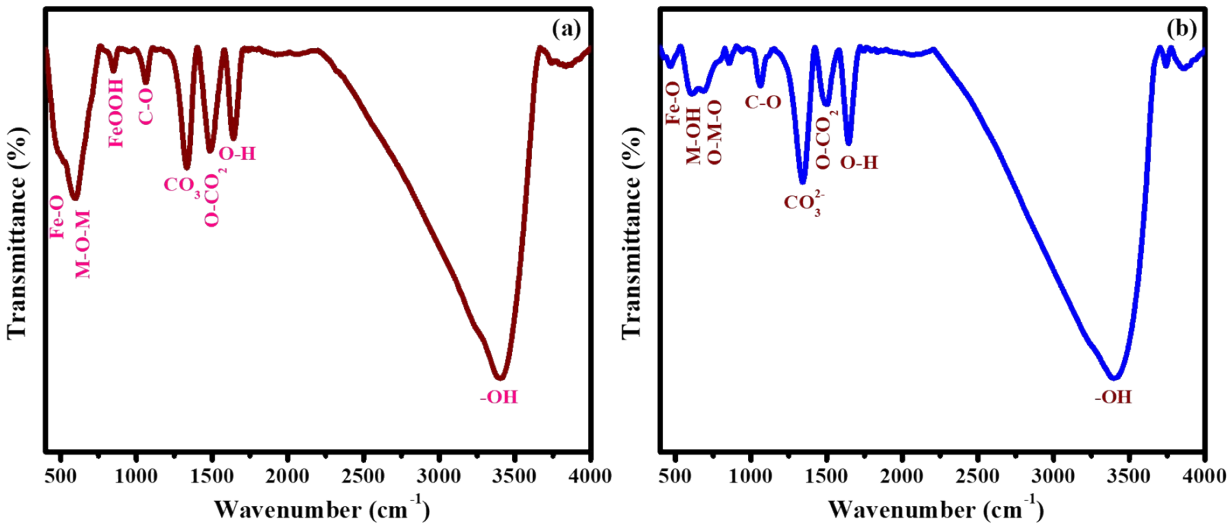

Figure S17. Post XPS Spectra of FeCoHS@NF; (a) Survey, (b) Iron and (c) Carbon.

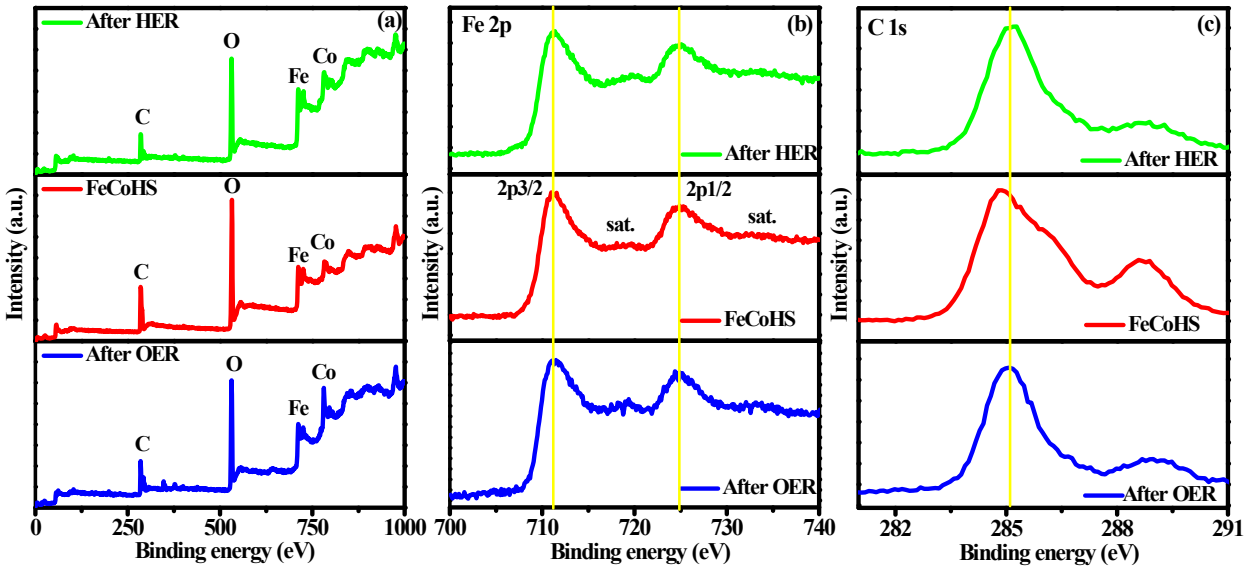

Figure S18. Post-OER XPS spectra of (a) oxygen, (b) cobalt, and post-HER XPS spectra of (c) oxygen, and (d) cobalt.

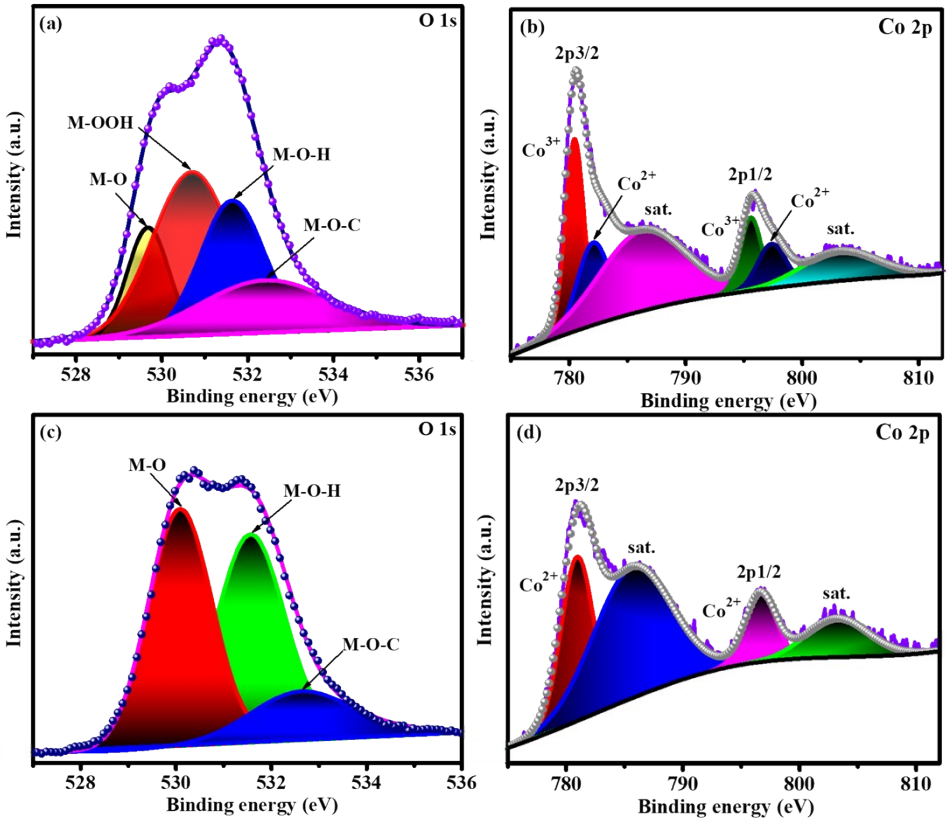

Figure S19. Solar cell FeCoHS@NF//FeCoHS@NF water electrolyzer for hydrogen production.

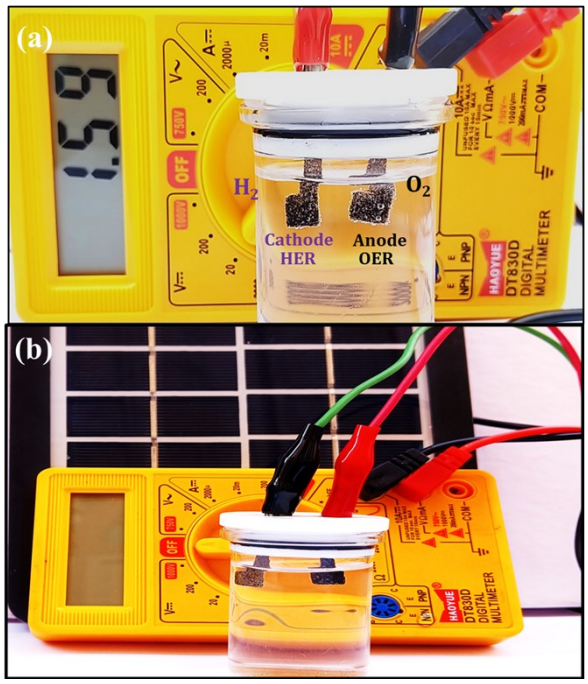

SI-IV. Tables

Table S1. Comparison of OER, HER and overall water splitting performance of FeCoHS with recently reported non-noble bifunctional electrocatalysts.

Electrolyte: 1 M KOH

S.No	Bifunctional Electrocatalyst	OER ηj=10 (mV)	HER ηj=10 (mV)	OWS Ej=10 (V)	Ref.
1	**FeCoHS@NF**	**250**	**130**	**1.59**	**This work**
2	Fe_2Co_8HCF	241	158	1.63	[2]
3	CP/CTs/Co-S	306	190	1.74	[3]
4	Co_1Mn_1CH/NF	294	180	1.68	[4]
5	$Co_2B/CoSe_2$	320	300	1.73	[5]
6	$Co_{0.85}Se$/NiFe-LDH/EG	270	260	1.67	[6]
7	Co $(OH)_2$@NCNTs	270	170	1.72	[7]
8	$Co(OH)_2$	281	182	1.65	[8]
9	Co_4Mo_2@NC	330	218	1.74	[9]
10	Co_2P/Mo_2C	368	182	1.74	[10]
11	Fe-PANI	261	155	1.64	[11]

Table S2. Comparison of overall Urea splitting performance of FeCoHS with recently reported non-noble bifunctional electrocatalysts.

S.No	Bifunctional Electrocatalyst	Electrolyte	OUS Ej=10 (V)	Ref.
1	**FeCoHS@NF**	**1.0M KOH + 0.33M urea**	**1.40**	**This work**
2	CoS_2NA/Ti	1.0M KOH + 0.3M urea	1.59	[12]
3	NiF_3/Ni_2P@CC-2	1.0M KOH + 0.33M urea	1.54	[13]
4	$Ni(OH)_2$-NiMoOx/NF	1.0M KOH + 0.5M urea	1.42	[14]
5	$CoMn/CoMn_2O_4$/NF	1.0M KOH + 0.5M urea	1.51	[15]
6	Mo-dopedNi3S2/NF	1.0M KOH + 0.3M urea	1.45	[16]
7	HC-NiMoS/Ti	1.0M KOH + 0.5M urea	1.59	[17]
8	FQD/CoNi-LDH/NF	1.0M KOH + 0.5M urea	1.45	[18]
9	Ni/C	1.0M KOH + 0.33M urea	1.60	[19]
10	Ni_3N NA/CC	1.0M KOH + 0.33M urea	1.44	[20]
11	Ru-$NiCo_2O_4$	.0M KOH + 0.33M urea	1.427	[21]

Table S3. Mass-based sustainability metrics evaluation for the synthetic process comparison with recently reported works.[22-25]

Material	Mass intensity (MI) (kg/kg)	Solvent intensity (SI) (kg/kg)	Reaction mass efficiency (RME) %	Energy consumption (kW·h/kg)	E-factor
FeCoHS@NF	1.29	38.7	77.6	2.5	0.3
NiFeHCF@NF	1.35	93.50	74	0	0.5
Fe-PANI	1.37	34.01	72.5	0	0.3
CNPFH	1.84	38.80	54	1.78	0.6
CMCFH	1.90	29.20	52	2.30	0.3

Table S4. Overall performance table.

Method	Electrolyte	Efficiency @ 10 mA/cm^2
Alkaline Water Electrolysis	1M KOH	OER-1.48 V HER-130 mV OWS-1.59 V
Urea-assisted Alkaline Water Electrolysis	1M KOH + 0.33 M Urea (natural Urea concentration in urea-polluted water)	UOR-1.23 V OUS-1.40 V
Alkaline Seawater Electrolysis	1M KOH + 0.5 M NaCl (natural NaCl concentration in seawater)	OER-1.47 V HER-130 mV OWS-1.54 V
Urea-assisted Seawater Electrolysis	1M KOH + 0.33 M Urea + 0.5 M NaCl (sewage water major contaminants)	OER-1.36 V OWS-1.49 V

SI-V. References

1 M. Zhong, M. Xu, S. Ren, W. Li, C. Wang, M. Gao and X. Lu, *Energy Environ. Sci.*, 2024, **17**, 1984–1996.

2 A. Gayathri, S. Mathi, M. Vijayarangan, J. Jayabharathi and V. Thanikachalam, *ChemistrySelect*, 2022, **7**, e202203616.

3 J. Wang, H. Zhong, Z. Wang, F. Meng and X. Zhang, *ACS Nano*, 2016, **10**, 2342–2348.

4 X.-D. Wang, H.-Y. Chen, Y.-F. Xu, J.-F. Liao, B.-X. Chen, H.-S. Rao, D.-B. Kuang and C.-Y. Su, *J. Mater. Chem. A*, 2017, **5**, 7191–7199.

5 Y. Guo, Z. Yao, C. Shang and E. Wang, *ACS Appl. Mater. Interfaces*, 2017, **9**, 39312–39317.

6 Y. Hou, M. R. Lohe, J. Zhang, S. Liu, X. Zhuang and X. Feng, *Energy Environ. Sci.*, 2016, **9**, 478–483.

7 P. Guo, J. Wu, X.-B. Li, J. Luo, W.-M. Lau, H. Liu, X.-L. Sun and L.-M. Liu, *Nano Energy*, 2018, **47**, 96–104.

8 S. Sriram, S. Mathi, B. Vishnu and J. Jayabharathi, *Energy Fuels*, 2022, **36**, 7006–7016.

9 J. Jiang, Q. Liu, C. Zeng and L. Ai, *J. Mater. Chem. A*, 2017, **5**, 16929–16935.

10 X. Li, X. Wang, J. Zhou, L. Han, C. Sun, Q. Wang and Z. Su, *J. Mater. Chem. A*, 2018, **6**, 5789–5796.

11 B. Vishnu, S. Sriram and J. Jayabharathi, *New J. Chem.*, 2023, **47**, 5977–5990.

12 S. Wei, X. Wang, J. Wang, X. Sun, L. Cui, W. Yang, Y. Zheng and J. Liu, *Electrochimica Acta*, 2017, **246**, 776–782.

13 K. Wang, W. Huang, Q. Cao, Y. Zhao, X. Sun, R. Ding, W. Lin, E. Liu and P. Gao, *Chem. Eng. J.*, 2022, **427**, 130865.

14 Z. Dong, F. Lin, Y. Yao and L. Jiao, *Adv. Energy Mater.*, 2019, **9**, 1902703.

15 C. Wang, H. Lu, Z. Mao, C. Yan, G. Shen and X. Wang, *Adv. Funct. Mater.*, 2020, **30**, 2000556.

16 H. Xu, Y. Liao, Z. Gao, Y. Qing, Y. Wu and L. Xia, *J. Mater. Chem. A*, 2021, **9**, 3418–3426.

17 X. Wang, J. Wang, X. Sun, S. Wei, L. Cui, W. Yang and J. Liu, *Nano Res.*, 2018, **11**, 988–996.

18 Y. Feng, X. Wang, J. Huang, P. Dong, J. Ji, J. Li, L. Cao, L. Feng, P. Jin and C. Wang, *Chem. Eng. J.*, 2020, **390**, 124525.

19 L. Wang, L. Ren, X. Wang, X. Feng, J. Zhou and B. Wang, *ACS Appl. Mater. Interfaces*, 2018, **10**, 4750–4756.

20 Q. Liu, L. Xie, F. Qu, Z. Liu, G. Du, A. M. Asiri and X. Sun, *Inorg. Chem. Front.*, 2017, **4**, 1120–1124.

21 Y. Wang, L. Chen, H. Zhang, M. Humayun, J. Duan, X. Xu, Y. Fu, M. Bououdina and C. Wang, *Green Chem.*, 2023, **25(20)**, 8181-8195.

22 A. Gayathri, V. Ashok, M. Sangamithirai, J. Jayabharathi and V. Thanikachalam, *Green Chem.*, 2024, **26**, 5326–5338.

23 S. Mukherjee, A. A. Kumar, C. Sudhakar, R. Kumar, T. Ahuja, B. Mondal, P. Srikrishnarka, L. Philip and T. Pradeep, *ACS Sustain. Chem. Eng.*, 2019, **7**, 3222–3233.

24 S. Mukherjee, H. Ramireddy, A. Baidya, A. K. Amala, C. Sudhakar, B. Mondal, L. Philip and T. Pradeep, *ACS Sustain. Chem. Eng.*, 2020, **8**, 139–147.

25 C. Jiménez-González, D. J. Constable and C. S. Ponder, *Chem. Soc. Rev.*, 2012, **41**, 1485–1498.